Formation of Bimetallic Ag−Pd Nanoclusters via the Reaction between Ag Nanoclusters and Pd^{2+} Ions

Ching-Hsiang Chen,[†] Loka Subramanyam Sarma,[†] Guo-Rung Wang,[†] Jiun-Ming Chen,[†] Shou-Chu Shih,[†] Mau-Tsu Tang,[‡] Ding-Goa Liu,[‡] Jyh-Fu Lee,[‡] Jing-Ming Chen,[‡] and Bing-Joe Hwang*[,†,‡]

Nanoelectrochemistry Laboratory, Department of Chemical Engineering, National Taiwan University of Science and Technology, Taipei 106, Taiwan, ROC, and National Synchrotron Radiation Research Center, Hsinchu 300, Taiwan

Received: February 21, 2006; In Final Form: April 3, 2006

We have investigated systematically the mechanistic aspects of the Ag−Pd bimetallic cluster formation within sodium bis(2-ethylhexyl)sulfosuccinate (AOT) reverse micelles by using in-situ X-ray absorption spectroscopy (XAS). A two-step sequential reduction method is employed for the synthesis of Ag−Pd bimetallic clusters. The first step involves preparation of Ag nanoclusters, by mixing the Ag^+ ions containing the AOT microemulsion system with a reducing agent hydrazine (N_2H_4) containing the AOT microemulsion system. In the second step, the addition of Pd^{2+} ions to Ag nanoclusters led to the formation of Ag−Pd bimetallic clusters via the reaction between Ag nanoclusters and Pd^{2+} ions in AOT reverse micelles. The reduction of silver ions and the formation of corresponding Ag nanoclusters are monitored as a function of the dosage of the reducing agent, hydrazine. In-situ XAS allowed probing of the reaction between Ag nanoclusters and Pd^{2+} ions during the formation of Ag−Pd bimetallic clusters. Analysis of Ag and Pd K-edge XAS spectra reveals that in the final stage Ag−Pd clusters, in which "Ag" atoms prefer to be surrounded by "Pd" and "Pd" atoms prefer to be surrounded by "Pd", were formed. On the basis of XAS results presented here, we are able to propose a structural model for each step so that this work provides a detailed insight into the mechanism of nucleation and growth of Ag−Pd bimetallic clusters. We also discussed the atomic distribution of Ag and Pd atoms in Ag−Pd bimetallic clusters based on the calculated XAS structural parameters.

Introduction

Nanoparticles exhibit novel material properties which largely differ from the bulk properties due to their smaller size and larger specific surface area.[1] Bimetallic nanoparticles (bi-MNPs) containing two metals are of great interest since they can exhibit catalytic, electronic, and optical properties distinct from those of corresponding monometal nanoparticles.[2] Due to their interesting physicochemical properties resulting from the combination of two kinds of metals, bi-MNPs synthesis, characterization, and screening for catalytic applications have been fascinating in the contemporary research. The materials synthesized from micellar solutions of surfactants, which combine the advantages of both high specific surface area and uniform particle size distribution, are of great interest for applications in catalysis and fuel cells. Since nanotechnology is regarded as a major future technology, methods of scaling-up nanoparticle synthesis are desired. Controlling the size, shape, and surface morphology are extremely important factors to study because these factors play pivotal roles in determining the physical, chemical, and optical properties of these nanoscopic materials.[3] It is believed that both for a successful particle design and for a scaling-up and also to control the morphology of nanoparticles a detailed knowledge of particle formation mechanism is needed. Hence new methods for understanding the formation of nanoparticles and the ability to tailor-make their size and shape have received considerable attention. Also studies on the reaction between nanoclusters and metal ions and their interactions is of great importance during the synthesis of metal-based nanoengineered clusters.[4] For example the formation of 1:6 Au−CdSe nanoclusters via the interaction between the Au nanoclusters and CdSe nanoclusters has been reported.[5] Judicious control of the nanocluster interaction parameters allows for control over the assembly of nanoparticles. Although a great wealth of research has been available in the literature on the synthesis and characterization of bi-MNPs,[6] efforts aimed at understanding the formation mechanism of bimetallic cluster interactions between nanoclusters and metal ions at early stages have been lacking until very recently.

One of the methods suitable to study the structure of metal clusters is the in-situ XAS (X-ray absorption spectroscopy).[7] The XAS method is especially interesting for investigating the environment of colloidal dispersions of very small metallic and bimetallic clusters, since it is difficult to obtain structural information on such clusters by conventional diffraction method at early stages. In addition, since the cluster structure would change during the course of formation, it is difficult to get the exact structural information in atmospheric conditions by using the ex-situ techniques such as transmission electron microscopy (TEM) and X-ray diffraction (XRD), and also TEM technique yields no information about the internal structure of nanoclusters. UV/vis spectroscopy can be applied in situ to get insights into the formation mechanism of both monometallic[8] and bimetallic nanoparticles.[9] By following Ag nonoparticle formation process in situ using UV/vis spectroscopy, Andersson et al.[8] have studied

* Corresponding author. Fax: +886-2-27376644. E-mail: bjh@mail.ntust.edu.tw.
[†] National Taiwan University of Science and Technology.
[‡] National Synchrotron Radiation Research Center.

10.1021/jp061095f CCC: $33.50
Published on Web 05/25/2006

the influence of silver ion and nonionic surfactants Brij30 and sodium bis(ethylhexyl)sulfosuccinate (AOT) on the formation kinetics. Liu et al.[9] have studied the Ag−Pd bimetallic nanoparticle formation process by using UV/vis spectroscopy, and they observed a characteristic absorption peak which is different not only from those of the monometallic Ag or Pd nanoparticles but also from those of their physical mixtures. This characteristic absorption peak is described as a result of overlap between the surface plasmon band of Ag and the interband transition of Pd.[9] Several researchers have taken these characteristic absorption spectra as evidence for the formation of Ag−Pd bimetallic nanoparticles.[10] Even though UV/vis spectroscopy gives information qualitatively about the formation of bimetallic NPs, however, it lacks identification of the short-range ordering and atomic-level understanding of the distribution of atoms inside the cluster. Furthermore, to better understand the structure−activity relationships of bimetallic NPs, it is necessary to understand the distribution of the two metal atoms within the individual nanoparticles, and studies focusing in this direction are highly needed. From an analysis of XAS data one can determine the local structure around a specific type of atom. It is possible to get information not only about the metal atoms surrounding a specific metal atom but also about the other atoms such as chlorine and oxygen, etc., surrounding the specific metal atom and distribution of metal atoms inside the cluster. In our previous studies the formation mechanism of Pt clusters,[11] Pt−Cu,[12] and Pd−Pt[13] in AOT reverse micelles has been successfully evaluated by means of in-situ X-ray absorption spectroscopy method. In line with our ongoing effort for the evaluation of the formation mechanism of metal nanoparticles, we have aimed here to probe in situ the reaction between Ag nanoclusters and Pd^{2+} ions and to deduce the formation mechanism of the resulting Ag−Pd bimetallic clusters in AOT reverse microemulsions by means of an XAS method. By analyzing the extended X-ray absorption fine structure (EXAFS) spectra of Ag−Pd bimetallic clusters at Ag K-edge and Pd K-edge, we are able to study the reaction of Ag nanoclusters and Pd^{2+} ions and proposed a formation mechanism of Ag−Pd nanoclusters by determining the variations of the parameters such as coordination number (N), bond distance (R), and static and dynamic disorder (σ_j^2) during the course of the reaction in the reverse microemulsion. A structural model was proposed for each step in the reduction process and atomic distribution of Ag and Pd inside the Ag−Pd bimetallic cluster is discussed on the basis of the XAS results. The methodology proposed in this contribution to study the formation mechanism would be beneficial to a rational design and size and shape control of metal nanoparticle fabrication, which is highly required for their superior catalytic activities.

Experimental Section

Synthesis of Ag Nanoclusters. Ag nanoclusters were prepared in microemulsions containing *n*-heptane as an oil component, water, and surfactant. The surfactant used was 1 M AOT. The *n*-heptane and the surfactant were thoroughly mixed, and an aqueous solution of 1 mL of 0.5 M $AgNO_3$ was subsequently added to form a microemulsion with Ag complex in the water pool to form a well-defined microemulsion phase. The volume ratio of aqueous phase to organic phase has been kept at 1:10. An important parameter characterizing the microemulsion, i.e., the water-to-surfactant molar ratio, $W_0 = [\text{water}]/[\text{surfactant}]$, was equal to 5.5 in the present experiment. This microemulsion solution was placed in a homemade liquid cell, which was carefully designed to avoid excessive attenuation of the X-ray beam. A microemulsion of the same composition of oil, water and the surfactant that contained 1 mL of 10 M hydrazine (N_2H_4) as reducing agent was also prepared. An appropriate amount of N_2H_4 containing microemulsion was then added to the $AgNO_3$-containing microemulsion using a microsyringe at different time intervals (0, 1.08, 3.08, 6.5, 11.85, and 13.52 h), whereby the Ag complex was reduced to Ag particles.

Synthesis of Ag−Pd Clusters in AOT Reverse Microemulsions. To the microemulsion containing Ag nanoclusters, 1 mL of 0.5 M $PdCl_2$ solution was added (at 16.33 h) to form Ag−Pd bimetallic clusters. All reactions were carried out at 298 K unless otherwise specified. Nitrogen gas was purged into the microemulsion system throughout the experiment to prevent the oxidation of nanoparticles by air.

In-Situ XAS Measurements. Pd K-edge and Ag K-edge XAS measurements were made at the BL12B2 station of Japan Synchrotron Radiation Research Institute (Spring-8), Japan. The Cl L-edge measurements were made at the BL20A1 station of Spring-8. The electron storage ring was operated at 8 GeV, and the ring current was 100 mA. A double Si (111) monochromator was employed for energy selection with a resolution of $\Delta E/E$ better than 1×10^{-4} at both Ag K-edge (25514 eV) and the Pd K-edge (24350 eV). Formation of Ag clusters and corresponding Ag−Pd bimetallic clusters in reverse micelles proceeded in a homemade cell made with poly(tetrafluoroethylene) (PTFE) for an in-situ XAS study. Two holes were made, one on top of the cell and the other on one side. After placing the liquid sample, the top hole was closed with a Teflon rod to avoid exposure of the sample to the outer atmosphere. A hollow Teflon rod with a Kapton film cap at one end was inserted into the outer hole in the in-situ cell. The position of the Teflon rod was adjusted to reach the optimum absorption thickness ($\Delta\mu x \approx 1.0$; $\Delta\mu$ is the absorption edge, and x is the thickness of the liquid layer) so that the proper edge jump could be achieved during the measurements. The monochromator was detuned by 10% to reject higher harmonics. Three ionization chambers were used in series to measure the intensities of the incident beam (I_0), the beam transmitted by the sample (I_t), and the beam subsequently transmitted by the reference foil (I_r). I_0 and I_t ion chambers were filled with a mixture of He + N_2 and Ar + N_2 for Ag K-edge measurement and with N_2 and Ar + N_2 for Pd K-edge, respectively. All the XAS measurements were carried out at room temperature. The Cl L-edge measurements were done in the total X-ray fluorescence yield mode with AgCl reference compound using an ultrahigh-vaccum chamber with a base pressure of 1×10^{-10} Torr. Both Ag and Pd experiments were done in the transmission mode with three detectors. The third detector was used in conjunction with the reference sample, which was a Ag foil in the case of Ag K-edge measurements and a Pd foil in the case of Pd K-edge measurements.

XAS Data Analysis. Standard procedures were followed to analyze the EXAFS data. First, the raw absorption spectrum in the preedge region was fitted to a straight line, and the background above the edge was fitted with a cubic spline. The EXAFS function, χ, was obtained by subtracting the postedge background from the overall absorption and then normalized with respect to the edge jump step. The normalized $\chi(E)$ was transformed from energy space to k space, where k is the photoelectron wave vector. The $\chi(k)$ data were multiplied by k^3 to compensate the damping of EXAFS oscillations in high-k region. Subsequently, k^3-weighted $\chi(k)$ data in the k space ranging from 3.18 to 10.33 $Å^{-1}$ and from 3.12 to 12.15 $Å^{-1}$ for Ag and Pd, respectively, was Fourier transformed (FT) to r

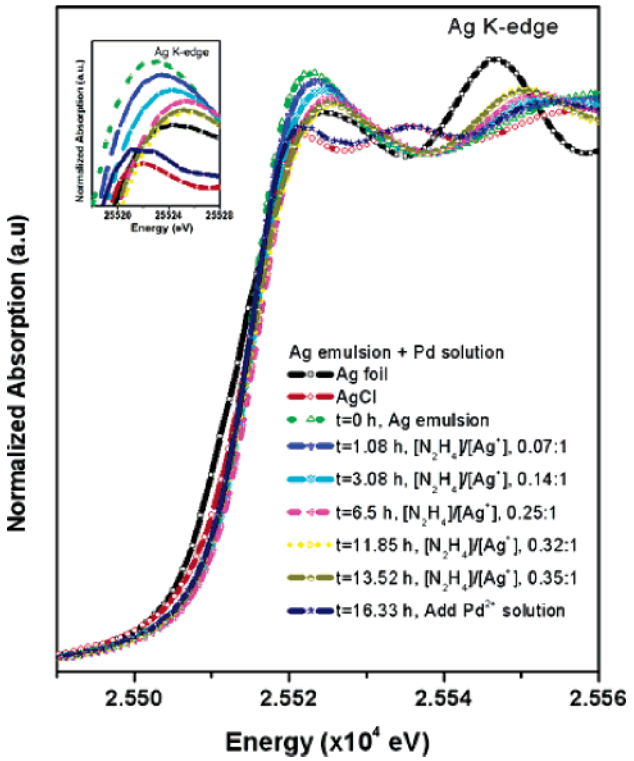

Figure 1. In-situ XANES spectra at Ag K-edge during the formation of Ag nanoclusters as a function of hydrazine dosage and the corresponding reaction of Ag nanoclusters with Pd^{2+} ions during the formation of Ag−Pd bimetallic clusters.

space in order to separate the EXAFS contributions from different coordination shells. A nonlinear least-squares algorithm was applied for curve- fitting of EXAFS in *r* space ranging from 1.51 to 3.18 Å and from 1.19 to 2 Å for Ag and Pd, respectively. All the computer programs were implemented in the UWXAFS 3.0 package[14] with the backscattering amplitude and the phase shift for a specific atom pair theoretically calculated by using the FEFF7 code.[15] Silver and palladium foils were employed as references for the Ag−Ag and Pd−Pd bonds. Ag−Pd is modeled with a *fcc* model containing six Ag and six Pd atoms in symmetric positions. The uncertainty in the coordination numbers (ΔN) is usually less than 20%. Following standards and criteria in XAS,[16] the error bars on fitted parameters can be estimated by using a standard statistical procedure.[17]

Results and Discussion

In-Situ X-ray Absorption Near-Edge Spectroscopy. *Formation of Ag Nanoclusters.* In XAS, the energy region in the vicinity of the absorption edge (0−50 eV) is referred to as X-ray absorption near-edge spectroscopy (XANES), and it is to a large extent a fingerprint for the oxidation state and site symmetry of the element from which the absorption spectrum was measured. Figure 1 shows the Ag K-edge XANES spectra recorded during the formation of Ag−Pd clusters in AOT reverse microemulsions as a function of the dosage of the reducing agent, N_2H_4. The XANES spectra recorded for the Ag foil standard and AgCl is also shown in Figure 1. It is believed that Ag nanocluster size, size distribution, shape, and structure made by the microemulsion technique are dependent on the formation and aggregation kinetics of a small silver cluster.[18] Hence control of these features is not trivial as Ag nanocluster reactions with Pd^{2+} ions depend on them.

As can be seen from Figure 1, at $t = 0$ h the Ag emulsion system shows a sharp peak on the rising edge at 25518 eV is assigned to the 1s → 5p transition.[19] The intensity of this peak (the so-called white line) is an immediate and definitive indication of the oxidation state of Ag. Hence, changes in the white line intensity/features of the spectrum indicate the changes in the oxidation state of Ag absorber. The white line intensity decreases as the molar ratio of N_2H_4 to Ag^+ increases from 0.07:1 to 0.14:1, indicating the reduction of Ag^{1+} ions. The features of the XANES spectra at the Ag K-edge of the Ag microemulsion system when the $[N_2H_4]/[Ag^+]$ ratio was at 0.25:1 at 6.5 h was found to be similar to that of the XANES spectra of reference Ag foil. No change in white line intensity was observed when the $[N_2H_4]/[Ag^+]$ ratio was increased to 0.35:1, and the XANES features exhibit identical oscillatory patterns characteristic of face-centered-cubic Ag.[20] It may indicate that all of the silver ions were completely reduced to Ag^0 and form Ag clusters. However, close examination of the XANES spectra reveals that the Ag clusters exhibit a small threshold shift to higher photon energy, and this may arise due to the size and surface effect of Ag clusters formed in the reverse microemulsion. The aim of progressive addition of the reducing agent over time is to control the reduction of metal ions and the size of metal particles at desirable sizes, since the size control of metal nanoparticles constitutes a crucial aspect of the synthetic process.[11−13]

Formation of Ag−Pd Clusters in AOT Reverse Microemulsions. After the addition of 1 mL of 0.5 M $PdCl_2$ solution into the microemulsion system at 16.33 h the white line intensity at the Ag K-edge has been decreased. Addition of $PdCl_2$ solution to the microemulsion containing Ag nanoclusters and trace amounts of hydrazine may lead to three possible reduction processes. One kind of possibility is that Pd^{2+} ions were reduced on Ag^0 nanoclusters and form $Ag_{core}-Pd_{shell}$ bimetallic nanoclusters. The second possibility is that part of the Ag^0 nanoclusters was oxidized and reacts with Cl^- ions to form AgCl clusters and the Pd^{2+} ions were reduced on the remaining Ag^0 clusters to form Ag−Pd nanoclusters. This kind of reaction is possible because the standard reduction potential of the Pd^{2+}/Pd pair (0.951 V vs SHE) is higher than that of the Ag^+/Ag pair (0.799 V vs SHE).[21] In this regard, Pd^{2+} ions were preferentially reduced as Pd^0 and the Ag^+ ions were formed due to the oxidation of Ag^0 clusters which are reactive toward Cl^- ions to form AgCl (solubility product value of AgCl, $K_{sp} = 1.8 \times 10^{-10}$). The last possibility is that Ag^0 nanoclusters may be completely oxidized in the solution to form AgCl clusters and Pd^{2+} ions were reduced to form isolated Pd clusters. Comparison of total electron mode XANES analysis at Cl $L_{II\&III}$-edge on dried sample obtained at the final step (5×10^{-4} M Pd^{2+} solution, 16.33 h) with the AgCl powder Cl $L_{II\&III}$-edge XANES spectra (Figure 2) revealed the presence of AgCl clusters in the final dried sample. However the possibilities of the AgCl presence in the solution or in the Ag−Pd or on the surface of Ag−Pd clusters cannot be simply realized from XANES spectra, and we will confirm the AgCl location after analyzing the EXAFS spectra in a later section.

Figure 3 shows the Pd K-edge region taken during the formation of Ag−Pd clusters from the microemulsion system containing Ag nanoclusters and Pd^{2+} ions. At the Pd K-edge, the first absorption transition at 24348 eV is a 1s → 4d dipole forbidden transition according to the selection rule, $\Delta l = 1$ and $\Delta j = 1$, where "*l*" is the orbital angular momentum and "*j*" is the total angular moment of the local density of states.[22] The second (24385 eV) and third (24435 eV) peaks correspond to dp and dsp transitions, respectively. As can be seen in Figure 3, soon after the addition of $PdCl_2$ solution to the microemulsion

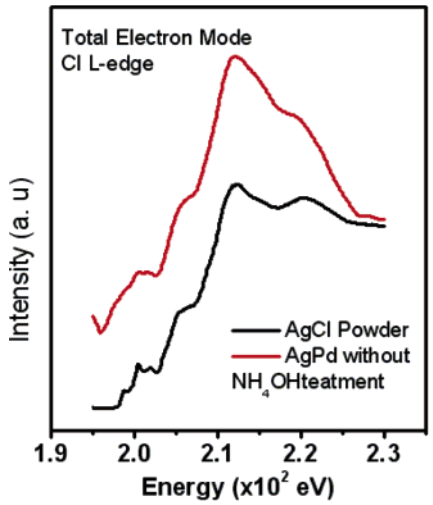

Figure 2. Total electron mode XANES spectra of the AgCl reference and the dried Ag−Pd bimetallic cluster sample at Cl $L_{II\&III}$-edge.

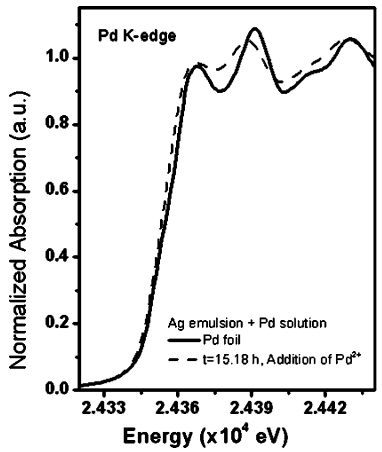

Figure 3. In-situ XANES spectra at Pd K-edge of the reaction between Ag nanoclusters with Pd^{2+} ions during the formation of Ag−Pd bimetallic clusters.

containing Ag nanoclusters the peak energy position is almost near the Pd foil. It was clearly observed that both the intensity and the shape of the white line of the near-edge spectra at the Pd K-edge were similar to that of Pd foil. Hence, these results clearly indicate the reduction of Pd^{2+} to Pd^0, and the coordination symmetry of Pd^0 clusters was similar to the Pd metal of the fcc structure.[23]

In-Situ Extended X-ray Absorption Fine Structure Spectroscopy. *Formation of Ag Nanoclusters.* Figure 4 shows the k^3-weighted EXAFS oscillations ($\Delta k = 3.18-10.33$ Å^{-1}) at Ag K-edge of Ag−Pd bimetallic cluster system. A high signal-to-noise ratio of the data allows EXAFS oscillations to be clearly observed up to 11 Å^{-1} and shows good data quality. It is found that the amplitude of oscillations increased with the increasing dosage of the reducing agent. Figure 5 shows Fourier transforms (k^3-weighted, $\Delta k = 3.18-10.33$ Å^{-1}) at Ag K-edge EXAFS of the Ag−Pd bimetallic cluster system as a function of the dosage of the reducing agent and time. Before the addition of reducing agent the FT of the Ag microemulsion exhibit a peak between 1.7 and 2.0 Å which can be attributed to the contribution of the Ag−O distances. When the molar ratio of $[N_2H_4]/[Ag^+]$ is at 0.07:1, the intensity of Ag−O is decreased and a new peak corresponds to the Ag−Ag shell that has appeared at 2.7 Å. When the dosage of the reducing agent increases, the intensity of Ag−Ag interactions increases.

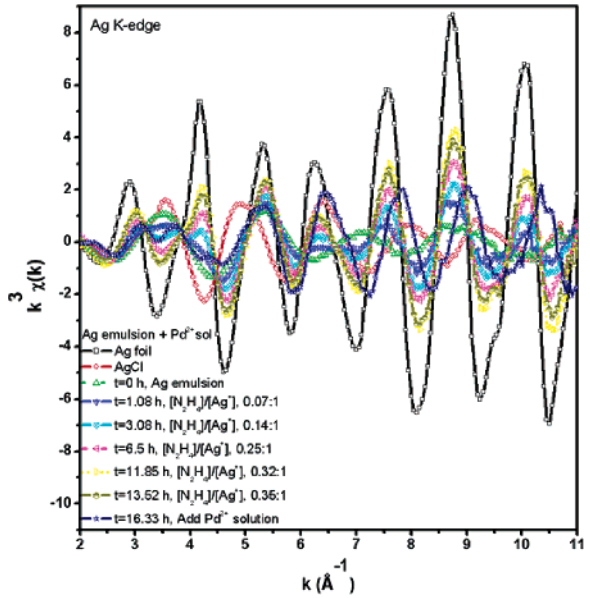

Figure 4. k^3-weighted EXAFS data at the Ag K-edge of the formation of Ag nanoclusters as a function N_2H_4 dosage and the corresponding reaction of Ag nanoclusters with Pd^{2+} ions during the formation of Ag−Pd bimetallic clusters.

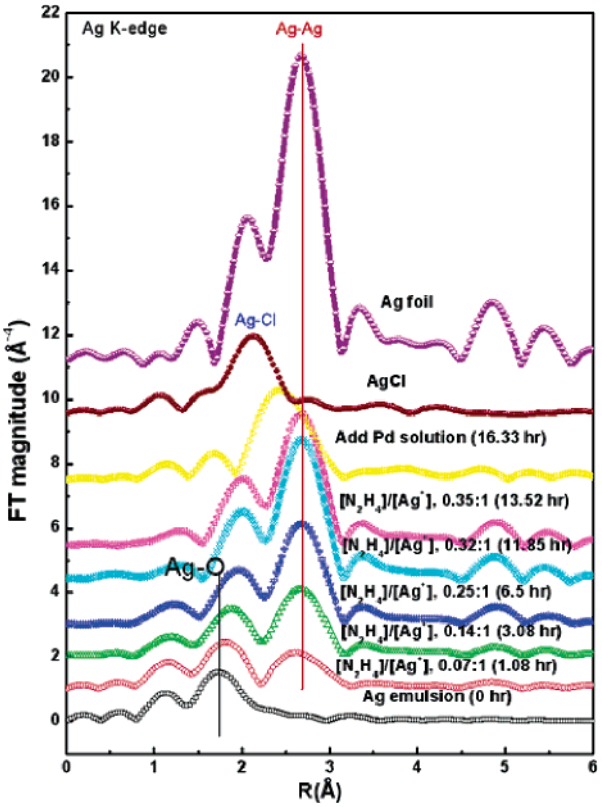

Figure 5. Fourier transforms of EXAFS spectra at the Ag K-edge of the formation of Ag nanoclusters as a function of the dosage of the reducing agent and the corresponding reaction of Ag nanoclusters with Pd^{2+} ions during the formation of Ag−Pd bimetallic clusters.

The structural parameters (coordination number, N; bond distance, R; Debye−Waller factor, σ^2; inner potential shift, E_0) were derived from the Ag K-edge EXAFS data analysis and are shown in Table 1. The coordination number N_{Ag-O} was found to be 0.8 in the absence of reducing agent. When the molar ratio of $[N_2H_4]/[Ag^+]$ is at 0.07:1 (1.08 h), N_{Ag-O} was found to be 0.7 and Ag−Ag coordination started to appear (N_{Ag-Ag}, 1.3), indicating the nucleation of Ag clusters. Further

TABLE 1: Structural Parameters (Coordination Number, *N*; Bond Distance, *R* ; Debye−Waller Factor, σ^2; Inner Potential Shift, ΔE_0) Derived from the Ag K-Edge EXAFS Data Analysis of the Ag−Pd Microemulsion System

		calculated parameters			
reducing agent dosage (mol)	shell	N	*R* (Å)	σ^2 ($\times 10^{-3}$) (Å^2)	ΔE_0 (eV)
0, 0 h	Ag−O	0.8(0.2)	2.03(0.02)	7.1(3.0)	33.55
3.52×10^{-5}, 1.08 h	Ag−O	0.7(0.2)	2.03(0.03)	6.3(4.5)	33.62
	Ag−Ag	1.3(0.7)	2.89(0.02)	8.9(4.0)	2.86
7.04×10^{-5}, 3.08 h	Ag−O	0.6(0.2)	2.03(0.02	6.1(4.0)	33.66
	Ag−Ag	2.6(0.6)	2.87(0.01)	9.7(2.0)	0.99
12.32×10^{-5}, 6.5 h	Ag−Ag	3.9(0.5)	2.86(0.01)	9.9(1.0)	−0.77
15.84×10^{-5}, 11.85 h	Ag−Ag	5.3(0.7)	2.86(0.01)	9.8(1.0)	−0.90
17.6×10^{-5}, 13.52 h	Ag−Ag	5.0(0.4)	2.86(0.01)	9.7(1.0)	−1.29
5×10^{-4} Pd^{2+} solution, 16.33 h	Ag−Cl	4.0(0.6)	2.69(0.02)	20.6(2.0)	−1.23
	Ag−Pd	1.9(0.3)	2.79(0.01)	8.8(1.0)	−3.14
after leaching the powder with 1 M NH_4OH	Ag−Pd	9.28(0.9)	2.78(0.01)	10.0(0.4)	−3.12
	Ag−Ag	0.83(0.3)	2.84(0.01)	0.1(0.8)	−3.12
Ag−Cl	Ag−Cl	4.3(0.9)	2.70(0.02)	15.8(1.3)	−3.23
Ag foil	Ag−Ag	12.0(1.1)	2.88(0.01)	9.2(1.0)	−2.18

increase of the molar ratio of $[N_2H_4]/[Ag^+]$ decreases the Ag−O coordination and increases the Ag−Ag interactions, indicating the growth of Ag clusters. The Ag−Ag coordination numbers are found to be 2.6, 3.9, and 5.3 respectively when the molar ratio of $[N_2H_4]/[Ag^+]$ is at 0.14:1 (7.08 h), 0.25:1 (6.5 h), and 0.32:1 (11.85 h). These observations indicate the reduction of Ag^+ ions and formation of Ag^0 clusters. The corresponding chemical reaction can be written as follows:

$$4Ag^+ + N_2H_4 \rightarrow 4Ag^0 + 4H^+ + N_2 \qquad (1)$$

Metallic nanoparticles prepared from micellar solutions are generally expected to possess uniform morphology.[11,12,24] The coordination numbers derived from XAS are a strong and nonlinear function of the particle diameter up to 3−5 nm. This property has been widely used in EXAFS analysis to determine the size of nanoparticles.[25] The particle size of the Ag clusters formed, calculated from the first shell coordination number, is about 1 nm.

Ag Nanoclusters Reaction with Pd^{2+} Ions during the Formation of Ag−Pd Bimetallic Clusters. After the addition of $PdCl_2$ solution into the microemulsion system containing Ag clusters and trace amounts of hydrazine, the position of the main FT peak is shifted to lower "R" values, indicating that the first coordination sphere of Ag atoms contains heteroatomic bonds. We found the contribution from Ag−Pd coordination at this stage (N_{Ag-Pd}, 1.9). We also found the contribution from Ag−Cl coordination at this stage (N_{Ag-Cl}, 4.0).

Figure 6 shows k^3-weighted Pd K-edge EXAFS spectra of the Ag−Pd bimetallic cluster system. Fourier transform was performed on the Pd K-edge EXAFS spectra in the 2.32−10.90 Å^{-1} region to obtain the radial distribution function (RDF) as shown in Figure 7. The main strong peak observed at 1.5−3 Å in the FT spectra (Figure 7) can be assigned to the Pd−Pd bond. The peak pattern of the Pd−Pd bond is close to the Pd−Pd bond of Pd foil. It indicates that soon after the addition of $PdCl_2$ solution into the microemulsion containing Ag nanoclusters, most of the Pd^{2+} ions are reduced to Pd^0. Because the size of the Ag nanoclusters, obtained from XAS results in the present investigation, is about 1 nm, the reactivity with Pd^{2+} ions is high. Moreover as we discussed in the XANES analysis at Ag K-edge during the formation of Ag−Pd clusters, that the standard reduction potential of the Pd^{2+}/Pd pair (0.951 V vs SHE) is greater than that of Ag^+/Ag pair (0.799 V vs SHE), hence Ag nanoclusters suspended in the solutions can be oxidized by $PdCl_2$ via the replacement reaction between Ag^0 and Pd^{2+} and the electron required for the reduction is contributed from the oxidation of Ag^0 to Ag^+. The corresponding chemical reaction can be written as follows:

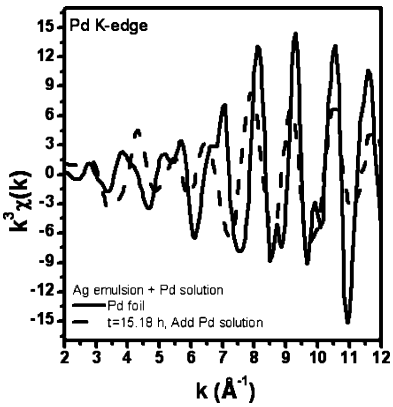

Figure 6. k^3-weighted EXAFS data at the Pd K-edge of the reaction between Ag nanoclusters with Pd^{2+} ions during the formation of Ag−Pd bimetallic clusters.

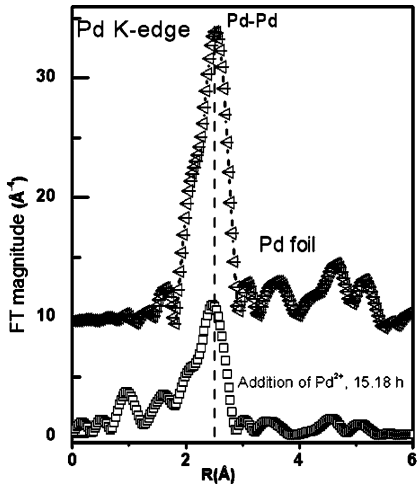

Figure 7. Fourier transforms of EXAFS spectra at the Pd K-edge of the reaction between Ag nanoclusters with Pd^{2+} ions during the formation of Ag−Pd bimetallic clusters.

$$3\,Ag^0 + PdCl_2 \rightarrow Ag{-}Pd^0 + 2AgCl \qquad (2)$$

The reduction of Pd^{2+}, Pt^{2+}, and Au^{3+} ions by Ag nanostructures is well-documented in the literature.[26−28] The possibility of nucleation of Pd and reduction of Pd^{2+} by hydrazine is less significant in the present investigation. The Ag K-edge XAS results show that soon after the addition of Pd^{2+} solution most of the Ag nanoparticles were oxidized, and from the Pd K-edge XAS one can see almost all of the Pd^{2+} ions were reduced to Pd. Moreover the amount of residual N_2H_4 (1.76×10^{-5} M) present in the system which corresponds to a $[N_2H_4]/[Pd^{2+}]$ molar ratio of 0.035:1 is far below the amount required to nucleate Pd. Also due to the instability of hydrazine, the amount may still be less than that of 1.76×10^{-5} M. In our earlier studies on formation of Pd/Pt bimetallic nanoclusters in AOT reverse micelles, we found that at least 26.4×10^{-5} M hydrazine is required for 0.6 M Pd^{2+} solution, which corresponds to a $[N_2H_4]/[Pd^{2+}]$ molar ratio of 0.4:1.[13] Hence we believe that the residual hydrazine if present is not sufficient to nucleate Pd. However, once Pd^{2+} ions are reduced, we can

TABLE 2: Structural Parameters (Coordination Number, *N*; Bond Distance. *R*; Debye−Waller Factor, σ^2; Inner Potential Shift, ΔE_0) Determined from the Analysis of Measured EXAFS Data at the Pd K-Edge of the Ag−Pd Bimetallic Cluster System

		calculated parameters			
reducing agent, N_2H_4 dosage (mol)	shell	N	R (Å)	σ^2 ($\times 10^{-3}$) (Å^2)	ΔE_0 (eV)
5×10^{-4} Pd^{2+} solution, 15.18 h	Pd−Pd	8.98(0.9)	2.75(0.007)	8.7(0.9)	−6. 7
	Pd−Ag	1.02(1.5)	2.83(0.130)	14.1(20.1)	19. 7
after leaching with 1 M NH_4OH	Pd−Pd	9.20(0.8)	2.77(0.006)	7.1(0.6)	−6. 6
	Pd−Ag	0.79(1.4)	2.88(0.140)	11.5(17.1)	20. 0
Pd foil	Pd−Pd	10.90(0.6)	2.75(0.002)	5.1(0.3)	1.8

speculate that the residual N_2H_4 may play a role in preventing substoichiometric amounts of Pd and the growth of corresponding Ag−Pd bimetallic clusters.

The structural parameters (N, R, σ^2, and E_0) were derived from the Pd K-edge EXAFS data analysis and are shown in Table. 2. The coordination number of Pd around Pd was found to be 8.98 soon after the addition of $PdCl_2$ solution to the microemulsion containing Ag clusters. All these XAS results indicate that the interaction of Ag nanocluster and Pd^{2+} ions in the microemulsion containing trace amounts of hydrazine produced Ag−Pd bimetallic nanoparticles.

Now we want to confirm whether the AgCl clusters formed are in the solution or embedded in the Ag−Pd cluster system. To do this, we have washed the final sample of Ag−Pd clusters containing Ag−Cl clusters with 1 M NH_4OH. It was reported in the literature that the Ag−Cl clusters can be removed by the formation of soluble complexes with different ligands using leaching systems such as $CS(NH_2)_2/H_2SO_4$, $Na_2S_2O_3$/NaOH, and NH_4OH.[29] Prior to XAS experiments, the sample was treated with 10% H_2 at 300 °C for 30 min. EXAFS spectra recorded at Ag K-edge and Pd K-edge for Ag−Pd bimetallic clusters after ammonia washings are shown in panels a and b of Figure 8. The EXAFS oscillation frequencies at both Ag K-edge and Pd K-edge of the Ag−Pd bimetallic clusters after the leaching process are different from that of Ag and Pd foils, indicating the existence of correlations between Ag and Pd.

Fourier transforms of Ag K-edge and Pd K-edge k^3-weighted EXAFS oscillations of Ag−Pd bimetallic clusters after leaching with ammonia are shown in the panels a and b, respectively, in Figure 9. As can be seen from Figure 9a, the FT peak related to the Ag−Ag coordination of the Ag−Pd bimetallic system matches well with that of the Ag−Ag peak of Ag foil and it was also observed that there is no contribution from Ag−Cl coordination. Similarly from Figure 9(b) the Pd−Pd FT peak of Ag−Pd bimetallic system was closely resembles that of the Pd−Pd peak of Pd foil. All these results indicate the formation of Ag−Pd bimetallic clusters free from Ag−Cl coordination. On the basis of the XAS results described above, we have shown in Figure 10 that the addition of Pd^{2+} salt solution to the microemulsion containing Ag nanoclusters and trace amounts of hydrazine led to oxidation of most of the Ag nanoclusters to Ag^+ and formation of AgCl and Pd^{2+} ions were reduced to Pd^0 on the remaining Ag nanoclusters to form Ag−Pd nanoclusters. The AgCl can be easily removed by leaching with 1 M ammonium hydroxide solution in order to get Ag−Pd nanoclusters free from AgCl.

We checked the reliability of the Ag−Pd and Pd−Ag bonds of Ag−Pd bimetallic clusters after ammonia washings by comparing the FEFF theoretical fit with the back-transformed experimental EXAFS data, and this is shown in panel a and b,

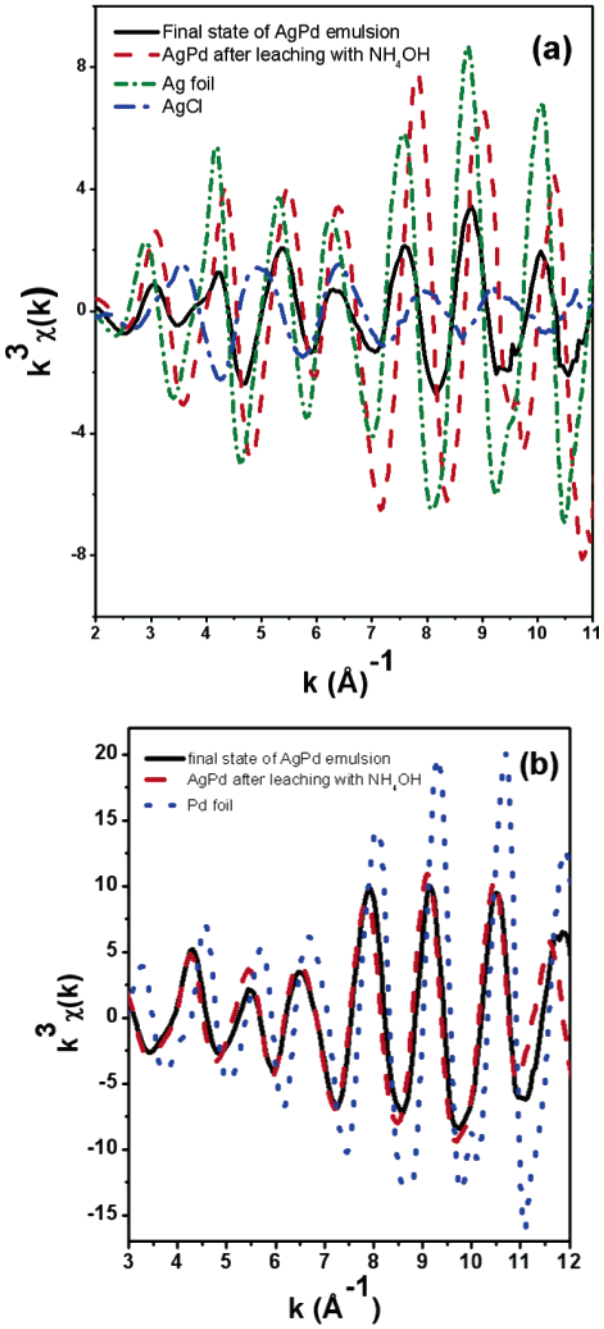

Figure 8. EXAFS spectra recorded for Ag−Pd bimetallic clusters after leaching with ammonia: (a) at the Ag K-edge and (b) at the Pd K-edge.

respectively, in Figure 11. The two-shell theoretical fit (dashed line) matches closely with the back-transformed experimental data of Figure 9 (solid line); good fit quality indicates that the Ag−Pd and Pd−Ag bonds are reliable.

Formation Mechanism of Ag Nanoclusters and Corresponding Ag−Pd Bimetallic Clusters in Reverse Microemulsion. On the basis of the XAS results described above, we are able to propose a formation mechanism of Ag nanoclusters and the corresponding reaction of Ag nanoclusters with Pd^{2+} ions during the formation of Ag−Pd bimetallic clusters. The formation of Ag−Pd clusters is observed step by step in this work, and a schematic representation of formation process is depicted in Scheme 1.

Five reaction steps of six stages were proposed in this model. In the initial stage (see stage I in the model) the microemulsion system contains Ag^+ ions, NO_3^- ions, and the SO_3^- group of

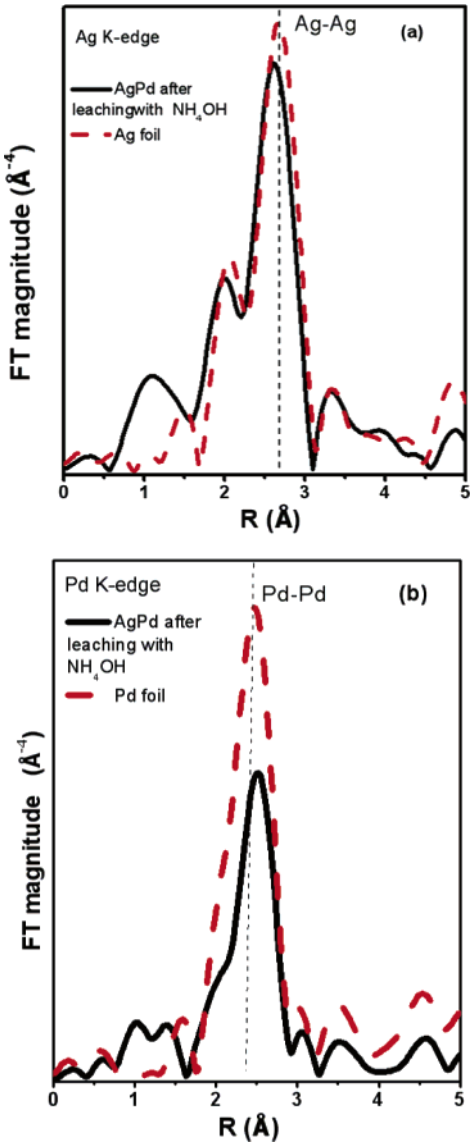

Figure 9. Fourier transformed EXAFS spectra of Ag−Pd bimetallic clusters after AgCl leaching with ammonia: (a) at the Ag K-edge and (b) at the Pd K-edge.

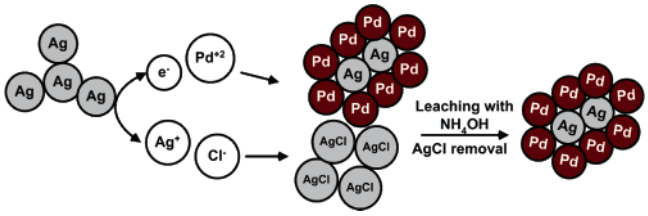

Figure 10. Schematic representation of the formation Ag−Pd and AgCl clusters and the removal of AgCl clusters.

the AOT surfactant. The Ag−O coordination number was around 0.8, and this would be due to Ag^+ ion coordination with the oxygen of either NO_3^- ions or the SO_3^- group of the AOT surfactant. When the molar ratio of N_2H_4 to Ag^+ is 0.07:1, in the first reaction step (reduction reaction, A), the Ag^+ ions started to reduce to form Ag^0 nuclei through intermicellar exchange processes (see stage II in the model).[30] Reverse micelles in solution will exchange the contents in their cores via both fusion and redispersion processes.[31] As a result, reduction of metal salt within the cores of the reverse micelles can result in the growth of nanosized metal particles. Subsequent particle growth depends strongly on exchange of the reactants

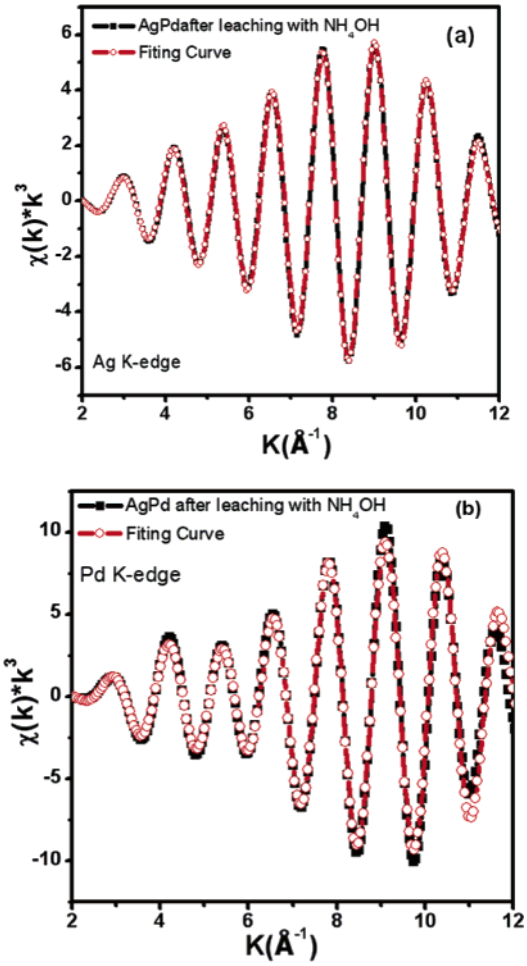

Figure 11. Two-shell fits (circle line) with back-transformed experimental EXAFS data of Figure 9 of Ag−Pd bimetallic clusters after ammonia washings: (a) at the Ag K-edge and (b) at the Pd K-edge.

between micelles. The exchange process occurs when micelles collide because of the Brownian motion or the attractive forces between the micelles. These collisions lead to a fusion of the reverse micelles, an exchange of the contents within the cores, and a redispersion of the micelles.[30,31] Further increase of the $[N_2H_4]/[Ag^+]$ molar ratio to 0.14:1 at 3.08 h in the second reaction step (growth reaction, B) increases the Ag−Ag coordination; however Ag−O coordination is still found in this reaction (see stage III in the model), indicating the growth of Ag nanoclusters. When the $[N_2H_4]/[Ag^+]$ molar ratio increased to 0.35:1 at 13.52 h in the third reaction step (Ag nanocluster formation reaction, C), Ag clusters were completely grown and the value of N_{Ag-Ag} was found to be 5.0 (see stage IV in the model). Addition of Pd^{2+} salt solution to the microemulsion containing Ag nanoclusters in the fourth reaction step resulted in formation of Ag−Pd clusters via the replacement reaction involving the oxidation of most of the Ag^0 nanoclusters to Ag^+ and reduction of Pd^{2+} to Pd^0 on the remaining Ag nanoclusters (reaction of Ag nanocluster with Pd^{2+} ions, D). The N_{Ag-Pd} and N_{Ag-Cl} was found to be 1.9 and 4.0, respectively (see stage V in the model). In fact the real coordination number of Pd around Ag is underestimated since Cl coordination is also used in the model. In this step from the Pd K-edge analysis the N_{Pd-Pd} and N_{Pd-Ag} was found to be 8.98 and 1.02, respectively. After ammonia washings in the final step (formation of pure Ag−Pd bimetallic clusters, E) the N_{Ag-Pd} and N_{Ag-Ag} was found to be 9.28 and 0.83, respectively. From the Pd K-edge the N_{Pd-Pd} and N_{Pd-Ag} was found to be 9.2 and 0.79, respectively. All these

SCHEME 1: Schematic of Formation Mechanism of Ag−Pd Bimetallic Clusters in AOT Reverse Microemulsions

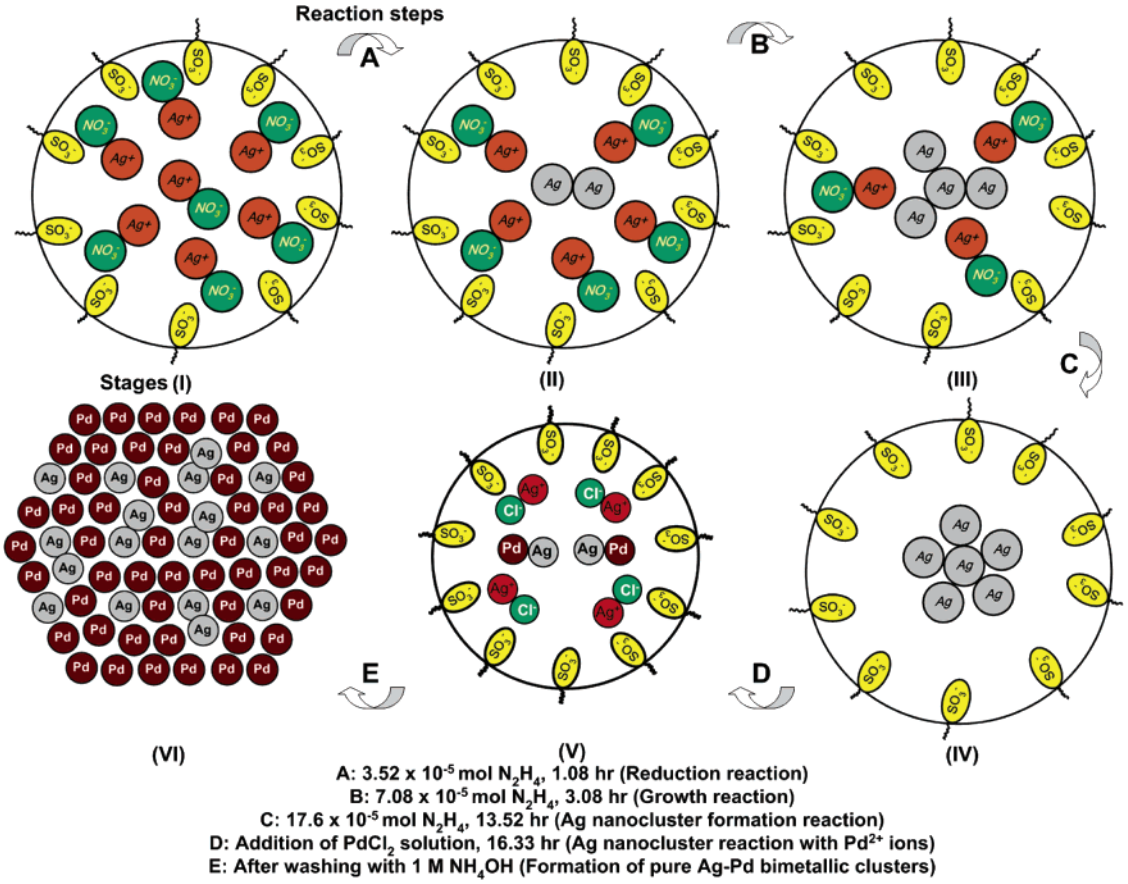

observations indicate the formation of Ag−Pd bimetallic clusters via the simultaneous reduction pathway (see stage VI in the model). In the resulting Ag−Pd clusters the total coordination number of Ag and Pd around absorbing "Ag" atoms ($N_{Ag-Ag} + N_{Ag-Pd}$, 10.11) is almost similar to the total coordination number of Pd and Ag atoms around absorbing "Pd" atoms ($N_{Ag-Ag} + N_{Ag-Pd}$, 9.99), indicating that the size of the Ag−Pd cluster is between 2 and 3 nm.

In our earlier studies on the Pt formation mechanism in AOT reverse micelles we found that the distribution of metal clusters obtained in microemulsions is of uniform size.[11] However, we found that the particle size obtained from TEM is larger than that obtained from XAS. This observation may be caused by the aggregation of nuclei due to the drying process during the TEM experiment. Due to this aggregation, the local structure of the cluster formed would definitely change. Hence, the exact structure of the cluster formed at the early stages is difficult to investigate by TEM measurements. Furthermore, it is also equally difficult to obtain structural information of nanoclusters by the conventional diffraction method at the early stage of formation since there is no long-range ordering in the nanoclusters at the early stage. Hence, studies on the mechanism of formation of Ag−Pd nanoclusters by in-situ X-ray absorption spectroscopy can offer the possibility to tailor their structure and size.

Composition and Atomic Distribution of Ag−Pd Bimetallic Clusters. The composition of the Ag−Pd cluster is calculated from XAS by measuring the edge jump at Ag K-edge and Pd K-edge and found that the atomic ratio of Ag:Pd is 0.35:1 ($Ag_{0.35}Pd$). It is satisfactory that the composition found from energy-dispersive X-ray (EDX) analysis (not shown here) is almost similar to the atomic ratio of Ag:Pd as 0.34:1 ($Ag_{0.34}$-Pd). Recently we have explored an XAS-based methodology to determine the alloying extent (or) atomic distribution of bimetallic nanoparticles.[32] We have applied this methodology for the Ag−Pd system investigated here. In the case of Ag−Pd bimetallic clusters after leaching with ammonia the Ag and Pd atoms around the Ag atom are found to be 0.83 and 9.28, respectively, and the total coordination number $\sum N_{Ag-i}$ is 10.11. The coordination numbers of Pd and Ag atoms around the Pd atom are determined as 9.20 and 0.79, respectively, and the total coordination number $\sum N_{Pd-i}$ is calculated as 10.01. From these values the structural parameters P_{obsd} ($N_{Ag-Pd}/\sum N_{Ag-i}$) and R_{obsd} ($N_{Pd-Ag}/\sum N_{Pd-i}$) were calculated as 0.92 and 0.078, respectively. The higher value of P_{obsd}, 0.92, indicates the higher extent of atomic dispersion of Ag′ atoms when compared to Pd. In other words the segregation of Pd atoms is more serious as the lower value of R_{obsd}, 0.078, suggests. The resulting Ag−Pd bimetallic clusters adopt a structure similar to the one shown in Scheme-1 (step VI) in which Ag atoms prefer to be surrounded by Pd atoms and Pd prefer to be surrounded by Pd atoms.

Conclusions

On the whole we found that the XAS methodology proposed here opens up new strategies and emerges as a good tool for the investigation of interactions between nanoclusters and ions and allows one to attain detailed insight into the mechanism of the nucleation and growth of bimetallic clusters. By using the experimental XAS data, we are able to propose a detailed model for the formation of Ag−Pd bimetallic clusters in AOT reverse microemulsions by probing the reaction between Ag nanoclusters and Pd^{2+} ions. The proposed possible structural models constructed for each step in the cluster formation process were reasonably explained by the XAS observations. In the resulting

Ag−Pd bimetallic clusters Ag atoms prefer to be surrounded by Pd atoms and Pd prefers to be surrounded by Pd atoms. On the basis of the XAS structural parameters, we found that atomic scale dispersion of Ag is much better than Pd, whereas in the case of Pd segregation effect dominates in the Ag−Pd bimetallic clusters of the present investigation. The proposed strategy is quite general and extendable for studying the other nanometallic clusters and metal ion interactions. An understanding of these interactions and their impact on the nanostructures is essential for initiating new synthetic methodologies of nanoengineered clusters.

Acknowledgment. We thank the National Science Council for financial support (under Contract Nos. NSC-93-2811-E-011-008, NSC-94-2214-E-011-010, and NSC-94-2120-M-011-002), and the facilities from the National Taiwan University of Science and Technology and the National Synchrotron Radiation Research (NSRRC) is gratefully acknowledged.

References and Notes

(1) (a) Toshima, N. In *Nanoscale Materials*; Liz-Marza'n, L. M., Kamat, P., Eds.; Kluwer: Norwell, MA, 2003; p 79. (b) Toshima, N.; Yonezawa, T. *New J. Chem*. **1998**, *22*, 1179. (c) Pileni, M. P. In *Metal Nanoparticles: Synthesis, Characterization, and Applications*; Feldheim, D. L., Foss, C. A., Jr., Eds.; Dekker: New York, 2001; p 207.

(2) Sinfelt, J. H. *Acc. Chem. Res*. **1987**, *20*, 134.

(3) (a) Link, S.; El-Sayed, M. A.; *J. Phys. Chem B* **1999**, *103*, 8410. (b) Petit, C.; Taleb, A.; Pileni, M. P. *Adv. Mater*. **1998**, *10*, 259.

(4) (a) Hirakawa, T.; Kamat, P. V. *J. Am. Chem. Soc*. **2005**, *127*, 3928. (b) Kim, H.; Achermann, M.; Balet, L. P.; Hollingsworth, J. A.; Klimov, V. I. *J. Am. Chem. Soc*. **2005**, *127*, 544.

(5) Cumberland, S. L.; Berrettini, M. G.; Javier, A.; Strouse, G. F. *Chem. Mater*. **2003**, *15*, 1047.

(6) (a) Torigoe, K.; Nakajima, Y.; Esumi, K. *J. Phys. Chem*. **1993**, *97*, 8304. (b) Toshima, N.; Harada, M.; Yonezawa, T.; Kushilhashi, K.; Asakura, K. *J. Phys. Chem*. **1991**, *95*, 7448. (c) Toshima, N.; Harada, M.; Yamazaki, Y.; Asakura, K. *J. Phys. Chem*. **1992**, *96*, 9927. (d) Liz-Marza'n, L. M.; Philipse, A. P. *J. Phys. Chem.* **1995**, *99*, 15120. (e) Yenezia, A.; Liotta, L.; Deganello, G.; Schay, Z.; Guczi, L. *J. Catal*. **1999**, *182*, 449. (f) Aihara, N.; Torigoe, K.; Esumi, K. *Langmuir* **1998**, *14*, 4945. (g) Damle, C.; Kumar, A.; Sastry, M. *J. Phys. Chem. B* **2002**, *106*, 297. (h) He, J.; Ichinose, I.; Kunitake, T.; Nakao, A.; Shiraishi, Y.; Toshima, N. *J. Am. Chem. Soc*. **2003**, *125*, 11034.

(7) (a) Hwang, B. J.; Tsai, Y. W.; Lee, J. F.; Borthen, P.; Strehblow, H. H. *J. Synchrotron Radiat*. **2001**, *8*, 484. (b) Borthen, P.; Hwang, B. J.; Strehblow, H. H.; Kolb, D. M. *J. Phys. Chem. B* **2000**, *104*, 5078.

(8) Andersson, M.; Pederson, J. S.; Palmqvist, A. E. C. *Langmuir* **2005**, *21*, 11387.

(9) Liu, H.; Mao, G.; Meng, S. *J. Mol. Catal.* **1992**, *74*, 275.

(10) (a) Torigoe, K.; Nakajima, Y.; Esumi, K. *J. Phys. Chem.* **1993**, *97*, 8304. (b) Torigoe, K.; Esumi, K. *Langmuir* **1993**, *9*, 1664. (c) D'souza, L.; Bera, P. Sampath, S. *J. Colloid Interface Sci.* **2002**, *246*, 92.

(11) Tsai, Y. W.; Tseng, Y. L.; Sarma, L. S.; Liu, D. G.; Lee, J. F.; Hwang, B. J. *J. Phys. Chem. B* **2004**, *108*, 8148.

(12) Hwang, B. J.; Tsai, Y. W.; Sarma, L. S.; Tseng, Y. L.; Liu, D. G.; Lee, J. F. *J. Phys. Chem. B* **2004**, *108*, 20427.

(13) Chen, C. H.; Hwang, B. J.; Wang, G. R.; Sarma, L. S.; Tang, M. T.; Liu, D. G.; Lee, J. F. *J. Phys. Chem B* **2005**, *109*, 21566.

(14) Stern, E. A.; Newville, M.; Ravel, B.; Yacoby, Y.; Haskel, D. *Physica B* **1995**, *208 and 209*, 117.

(15) Zabinsky, S. I.; Rehr, J. J.; Ankudinov, A. L.; Albers, R. C.; Eller, M. J. *Phys. Rev. B* **1995**, *52*, 2995.

(16) Lytle, F. W.; Sayers, D. E.; Stern, E. A. *Physica B* **1989**, *158*, 701.

(17) Bevington, P. R. *Data Reduction and Error Analysis for the Physical Sciences*; McGraw-Hill: New York, 1992; p 205.

(18) Zhang, Z. Q.; Patel, R. C.; Kothari, R.; Johnson, C. P.; Friberg, S. E.; Aikens, P. A. *J. Phys. Chem. B* **2000**, *104*, 1176.

(19) Allen, P. G.; Gash, A. E.; Dorhout, P. K.; Strauss, S. H. *Chem. Mater*. **2001**, *13*, 2257.

(20) Coulthard, I.; Sham, T. K. *Phy. Rev. Lett*. **1996**, *77*, 4842.

(21) *CRC Handbook of Chemistry and Physics*, 80th ed.; Lide, D. R., Ed.; CRC Press: Boca Raton, FL, 1999−2000; p 8.

(22) Choi, S. J.; Kang, S. K. *Catal. Today* **2004**, *93*−*95*, 561.

(23) Okamoto, K.; Akiyama, R.; Yoshida, H.; Yoshida, T.; Kobayashi, S. *J. Am. Chem. Soc*. **2005**, *127*, 2125.

(24) (a) Chen, D. H.; Yeh, J. J.; Huang, T. C. *J. Colloid Interface Sci.* **1999**, *215*, 159. (b) Wu, M. L.; Chen, D. H.; Hwang, T. C. *Chem. Mater*. **2001**, *13*, 599. (c) Wu, M. L.; Chen, D. H.; Hwang, T. C. *J. Colloid Interface Sci*. **2001**, *243*, 102.

(25) (a) Frenkel, A. I.; Hills, C. W.; Nuzzo, R. G. *J. Phys. Chem. B* **2001**, *105*, 12689. (b) Shibata, T.; Bunker, B. A.; Zhang, Z.; Meisel, D.; Vardeman, C. F., II; Gezelter, D. *J. Am. Chem. Soc.* **2002**, *124*, 11989. (c) Via, G. H.; Sinfelt, J. H.; Lytle, F. W. *J. Chem. Phys.* **1979**, *71*, 690. (d) Greegor, R. B.; Lytle, F. W. *J. Catal*. **1980**, *63*, 476.

(26) Sun, Y.; Mayers, B. T.; Xia, Y. *Nano Lett*. **2002**, *2*, 481.

(27) Sun, Y.; Mayers, B.; Xia, Y. *Adv. Mater*. **2003**, *15*, 641.

(28) Selvakannan, P. R.; Sastry, M. *Chem. Commun*. **2005**, *13*, 1684.

(29) Maudos, I.; Chimenon, J. M.; Segama, M.; Espiell, F. *Hydrometallurgy* **1996**, *40*, 153.

(30) (a) Hirai, T.; Sato, H.; Komasawa, I. *Ind. Eng. Chem. Res.* **1994**, *33*, 3262. (b) Bagwe, R. P.; Khilar, K. C. *Langmuir* **1997**, *13*, 6432.

(31) (a) Petit, C.; Jain, T. K.; Billoudet, F.; Pileni, M. P. *Langmuir* **1994**, *10*, 4446. (b) Towey, T. F.; Khan-Lodhi, A.; Robinson, B. H. *J. Chem. Soc., Faraday Trans.* **1990**, *86*, 3757. (c) Joshi, S. S.; Patil, S. F.; Iyer, V.; Mahumuni, S. *Nanostruct. Mater.* **1998**, *10*, 1135.

(32) Hwang, B. J.; Sarma, L. S.; Chen, J. M.; Chen, C. H.; Shih, S. C.; Wang, G. R.; Liu, D. G.; Lee, J. F. Tang, M.-T. *J. Am. Chem. Soc.* **2005**, *127*, 11140.